JACS
JOURNAL OF THE AMERICAN CHEMICAL SOCIETY
Article
pubs.acs.org/JACS

The Homogeneous Reduction of CO_2 by [Ni(cyclam)]$^+$: Increased Catalytic Rates with the Addition of a CO Scavenger

Jesse D. Froehlich and Clifford P. Kubiak*

Department of Chemistry and Biochemistry, University of California, San Diego, 9500 Gilman Drive, La Jolla, California 92093-0358, United States

Supporting Information

ABSTRACT: The homogeneous electrochemical reduction of CO_2 by the molecular catalyst [Ni(cyclam)]$^{2+}$ is studied by electrochemistry and infrared spectroelectrochemistry. The electrochemical kinetics are probed by varying CO_2 substrate and proton concentrations. Products of CO_2 reduction are observed in infrared spectra obtained from spectroelectrochemical experiments. The two major species observed are a Ni(I) carbonyl, [Ni(cyclam)(CO)]$^+$, and a Ni(II) coordinated bicarbonate, [Ni(cyclam)(CO_2OH)]$^+$. The rate-limiting step during electrocatalysis is determined to be CO loss from the deactivated species, [Ni(cyclam)(CO)]$^+$, to produce the active catalyst, [Ni(cyclam)]$^+$. Another macrocyclic complex, [Ni(TMC)]$^+$, is deployed as a CO scavenger in order to inhibit the deactivation of [Ni(cyclam)]$^+$ by CO. Addition of the CO scavenger is shown to dramatically increase the catalytic current observed for CO_2 reduction. Evidence for the [Ni(TMC)]$^+$ acting as a CO scavenger includes the observation of [Ni(TMC)(CO)]$^+$ by IR. Density functional theory (DFT) calculations probing the optimized geometry of the [Ni(cyclam)(CO)]$^+$ species are also presented.

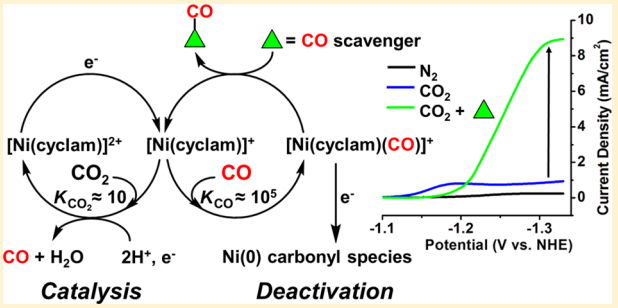

INTRODUCTION

The electrochemical reduction of CO_2 to higher energy products has received considerable attention recently.[1−3] The majority of the well-studied systems produce CO or formate as the major reduced product. These are considered to be intermediates on the path to liquid fuels. Utilizing CO_2 as a feedstock to create liquid fuel would both help to alleviate our dependence on fossil fuels as well as help mitigate rising atmospheric CO_2 levels by creating a carbon neutral source of combustible energy.

The heterogeneous reduction of CO_2 by metallic electrodes has been explored;[4] however, the mechanisms of these systems can be difficult to study and often suffer from poisoning of the electrode by the intermediates or products of catalysis.[5] Transition metal molecular catalysts can be used in a homogeneous fashion by acting as an electron shuttle between an electrode and CO_2 in solution. The molecular catalyst serves to stabilize intermediate species allowing for less negative potentials to be used in the reduction of CO_2. In addition, these intermediates can be characterized with solution based techniques not available to heterogeneous systems, thereby providing more mechanistic insight into the reduction of CO_2.

Many different molecular catalyst systems have been studied and can be found in recent reviews.[6−9] Many of these utilize expensive, rare earth metals. There are several notable catalysts that contain abundant first row transition metals such as Mn, Fe, Co and Ni.[6,10−12] Several of these systems were shown to have high selectivity for CO_2 reduction (rather than proton reduction) in organic solvents with added proton sources. Molecular catalysts that contain earth-abundant metal centers and operate in aqueous solutions with high efficiency, turnover rates, and selectivity are rare. The macrocyclic complex, [Ni(cyclam)]$^{2+}$ (cyclam = 1,4,8,11-tetraazacyclotetradecane) and its analogues, is one such example that has been extensively studied.[13−15] This molecular catalyst system has the unique ability to maintain efficient production of CO in an aqueous solution; however, the overwhelming majority of these studies use a mercury (Hg) working electrode. Hg has a very negative potential for proton reduction giving it an extensive negative potential solvent window in water making it a popular electrode choice for aqueous reduction electrochemistry. Furthermore, [Ni(cyclam)]$^+$ has been shown to adsorb onto the Hg surface, which enhances its catalytic activity for CO_2 reduction.[14,16] Our group's recent work demonstrated that [Ni(cyclam)]$^+$ still has considerable catalytic activity for CO production at an inert glassy carbon electrode.[17] The homogeneous (Hg free) reduction of CO_2 by [Ni(cyclam)]$^+$ has not been thoroughly explored and is the subject of the present study.

EXPERIMENTAL PROCEDURES

Cyclic voltammetry was performed on a Gamry Reference 600 potentiostat with a glassy carbon (GC) working electrode, platinum counter and Ag/Ag$^+$ (BASi) reference electrode separated by a piece of vycor glass. 0.1 M tetrabutylammonium hexafluorophosphate ($TBAPF_6$) was used as the electrolyte in all cyclic voltammetry and spectroelectrochemical experiments. All cyclic voltammogram poten-

Received: December 17, 2014
Published: February 25, 2015

DOI: 10.1021/ja512575v
J. Am. Chem. Soc. 2015, 137, 3565−3573

tials were converted to normal hydrogen electrode (NHE) reference by adding 0.54 V.

The acetonitrile (ACN) used was dried over basic alumina with a custom dry solvent system. The CO_2 used was flowed through a column packed with Drierite during sparging. Under 1 atm, the concentration of CO_2 in saturated aqueous[18] and ACN[19] solutions are reported as 0.036 and 0.28 M, respectively. The concentration of CO_2 in a 1:4 water:ACN mixed solvent system is estimated to be ≈190 mM.[20] The concentration of CO in saturated aqueous[18] and ACN[19] solutions are reported as 0.001 and 0.0083 M, respectively. The concentration of CO in a 1:4 water:ACN mixed solvent system is estimated to be ≈6 mM. The CO_2 concentration study utilized a flow meter system with the flow rates Ar and CO_2 controlled and then mixed. The gas mixture was then flowed through an ACN solution and then into a sparging needle in the cyclic voltammogram (CV) cell so as to minimize solvent evaporation. The ratio of the flow rate of the two gases was used to calculate the equilibrium concentration of CO_2 in solution. (***Warning**: Small amounts of highly toxic $Ni(CO)_4$ can be generated during the reduction of Ni complexes in the presence of CO.*)

A schematic of the infrared-spectroelectrochemistry (IR-SEC) setup used can be seen in a recent report.[21] The electrodes in the IR-SEC cell consist of a glassy carbon disk for the working electrode, a platinum counter and a silver quasi-reference. IR-SEC samples were prepared in a dry/N_2 glovebox by bubbling 10 mL of CO_2 through a 1 mL solution of the Ni(II) species and 0.1 M $TBAPF_6$ and injecting into the IR-SEC cell. The IR used was a Thermo Scientific Nicolet 6700 FT-IR. The potential was held for 10 s before the IR scan was initiated. The scans (16 scans) were completed in roughly 90 s.

RESULTS AND DISCUSSION

Electrochemistry. The cyclic voltammetry (CV) of $[Ni(cyclam)]^{2+}$ in an aqueous and mixed aqueous/acetonitrile solvent has been reported previously.[17] The mixed solvent system is convenient because the Ni(II)/Ni(I) couple is observable at a glassy carbon electrode whereas in an all aqueous system, without addition of CO_2, the reduction couple is obscured by the solvent window (proton reduction). After saturation with CO_2 both the aqueous and mixed solvent systems show high Faradaic efficiencies for CO production suggesting the active catalyst in the Ni(I) reduced state preferentially reacts with CO_2 rather than protons. Although, in highly acidic solutions H_2 production dominates over CO production.

The overall mechanism for CO_2 reduction by $[Ni(cyclam)]^{2+}$ is summarized in Scheme 1.[14] The Ni center is first reduced to generate the active catalyst, $[Ni(cyclam)]^{+}$, which in turn can react with CO_2. In the presence of a proton source, significant catalytic current is observed. In order to further investigate the mechanism of CO_2 reduction, the electrochemistry was studied in a proton-free organic solvent system and CO_2 and proton concentration studies were undertaken.

Scheme 1. Proposed CO_2 Reduction Catalytic Cycle for $[Ni(cyclam)]^{2+}$

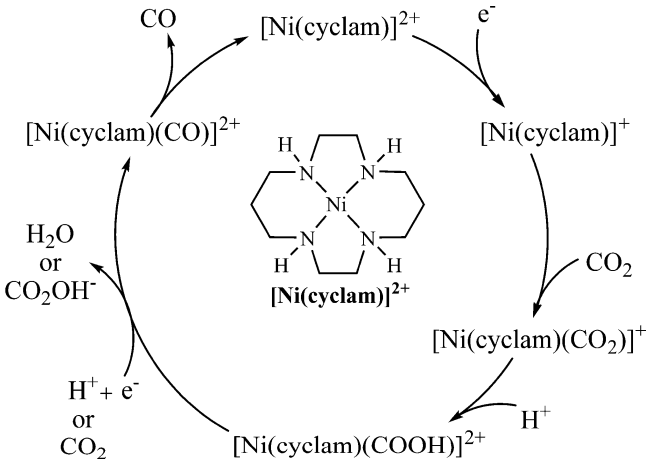

Electrochemistry in the Absence of Added Protons. The CV of $[Ni(cyclam)]^{2+}$ in acetonitrile (ACN) under N_2 and CO_2 can be seen in Figure 1. With the addition of CO_2 to the

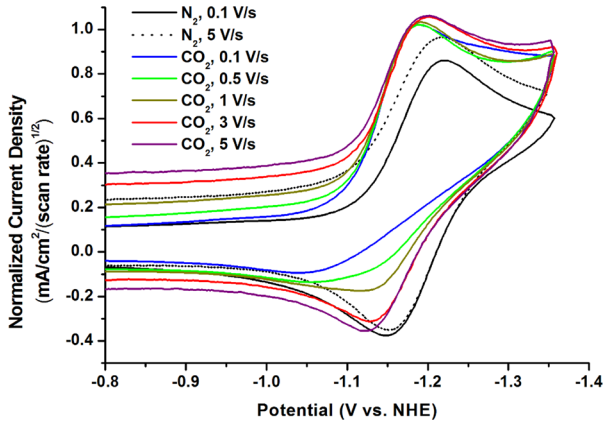

Figure 1. Cyclic voltammograms of 1 mM $[Ni(cyclam)](PF_6)_2$, 0.1 M $TBAPF_6$ in ACN. Current normalized by square root of scan rate.

$[Ni(cyclam)]^{2+}$ solution in ACN the Ni(II)/Ni(I) redox couple becomes irreversible and the reduction peak has a slight increase in current and is shifted positively by 30 mV. The positive shift is due to CO_2 binding to Ni(I). The irreversibility may arise from two possibilities: (1) CO_2 binding is an irreversible process, or (2) there is a fast, irreversible chemical step (eq 2) following CO_2 binding or an ECC mechanism. Possibility (1) may be ruled out by consideration of the fast kinetics of CO_2 binding. Kelly et al. reported the kinetics for the process shown in eq 1 in aqueous solution to be $k_f = 3.2 \times 10^7$ M^{-1} s^{-1} and $k_r = 2.0 \times 10^6$ s^{-1} for the forward and reverse reactions, respectively.[22] These rate constants imply that CO_2 binding is a reversible process on the time scale of CV. For possibility (2), the fast, irreversible chemical step following CO_2 binding could be an isomerization or protonation. It has been reported that reduction of a divalent Ni complex was accompanied by an isomerization process.[23] If it is due to a protonation step, the protons would have to come from the electrolyte, solvent, residual water or [Ni(cyclam)] amine protons.

$$[Ni(cyclam)]^{+} + CO_2 \rightleftharpoons [Ni(cyclam)(CO_2)]^{+} \quad (1)$$

$$[Ni(cyclam)(CO_2)]^{+} \rightarrow \text{intermediate} \quad (2)$$

Interestingly, a reversible couple can be obtained under CO_2 at faster scan rates. Figure 1 also shows the CV of $[Ni(cyclam)]^{2+}$ under CO_2 at various scan rates. Reversibility of the Ni(II)/Ni(I) couple is regained with scan rates above 3 V/s. With a reversible couple, the CO_2 binding constant (K_{CO_2}) can be calculated from the shift in the Ni(II)/Ni(I) couple (ΔE) under N_2 and CO_2 and eq 3.[24]

$$K_{CO_2}[CO_2] = e^{\Delta E(nF/RT)} - 1 \quad (3)$$

DOI: 10.1021/ja512575v
J. Am. Chem. Soc. 2015, 137, 3565−3573

Using this electrochemical determination method K_{CO_2} was found to be 6 M^{-1}, which is in very good agreement with the previous reported value (4 ± 2 M^{-1}).[25] In addition to an equilibrium constant, information about the rate of the chemical step following CO_2 binding can be obtained. Assuming that with faster scan rates the chemical step (eq 2) cannot proceed because the Ni(I) metal center is reoxidized to Ni(II) before the system can reach equilibrium, the half-life ($t_{1/2}$) is estimated to be ≈0.2 s under these conditions. It should be noted that if water is added to the solution the reversibility is lost even at higher scan rates (Figure S1). This suggests that the chemical step responsible for irreversibility is most likely protonation of the CO_2 adduct. Even though care was taken to exclude water from the electrolyte solution by solvent purification and drying of the CO_2 stream used, there is probably water in concentrations in excess of the catalyst in solution (>1 mM). The oxygens of the CO_2 adduct would be basic in nature and are capable of abstracting a proton under these conditions, especially if a proton-coupled electron transfer (PCET) mechanism is invoked. A recent computational study concluded that PCET is the most likely mechanism for the protonation of the CO_2 adduct at the moderate potentials where catalysis is observed.[26]

Electrochemistry with Added Protons. It is clear from the lack of significant catalytic current (i_{cat}) in ACN that high turnover frequencies (TOF) are not possible without the addition of a proton source. Multiple turnovers are not possible if relying only on trace water content in the ACN and no clear additional reduction peaks are observed without added water indicating that the unprotonated CO_2 adduct is not reduced at these potentials. Figure 2 shows CVs with increasing amounts

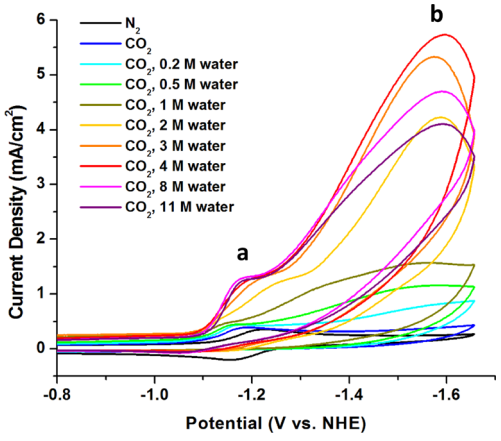

Figure 2. Effect of added H_2O on the cyclic voltammogram. 1 mM $[Ni(cyclam)](PF_6)_2$, 0.1 M $TBAPF_6$ in ACN saturated with CO_2. Additions of aqueous 1 mM $[Ni(cyclam)](PF_6)_2$ in order to maintain constant catalyst concentration. Scan rate = 0.1 V/s.

of water as the proton source. As water is added, two catalytic peaks develop. The first catalytic peak, **a**, simultaneously increases in current density and shifts positively in potential suggesting a proton dependent electron transfer. This agrees with the reported mechanism in which the second reduction occurs only after protonation of the CO_2 adduct.[14] At a water concentration of 4 M peak **a** approaches the same potential as the $[Ni(cyclam)]^{2+}$ reduction peak under CO_2 (−1.19 V vs NHE). The second catalytic peak, **b**, increases reaching a maximum current density and a peak potential of −1.59 V at ≈4 M water, then slightly decreasing at 11 M water. The current in peak **b** is assumed to be, in part, the reduction of a $[Ni(cyclam)(CO)]^+$ species produced by reaction of $[Ni(cyclam)]^+$ with CO. Additional contributions to the current in **b** could also be from CO_2 or proton reduction by a Ni(0) species or at the electrode. Evidence of $[Ni(cyclam)(CO)]^+$ forming during CO_2 reduction by $[Ni(cyclam)]^+$ has been reported previously on a Hg electrode.[14]

Further information on the nature of the second catalytic peak, **b**, can be obtained by varying the CO_2 concentration. Figure 3 shows the CV of 5 mM $[Ni(cyclam)]^{2+}$ in a 1:4

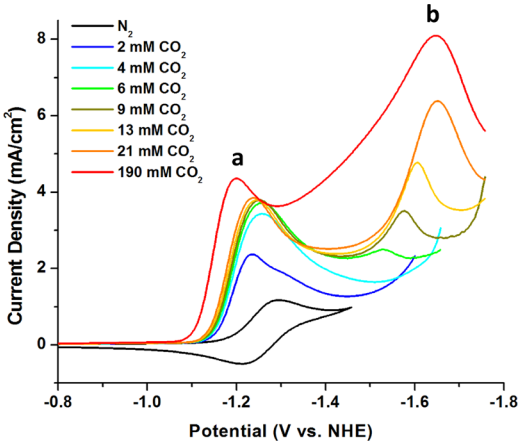

Figure 3. Cyclic voltammograms of 5 mM $[Ni(cyclam)](Cl)_2$, 0.1 M $TBAPF_6$ in 1:4 water:ACN. Adding CO_2 with flow meter. The positive scan portion has been removed for clarity. Scan rate = 0.1 V/s.

water:ACN solution. The first catalytic peak, **a**, quickly reaches a plateau as the CO_2 concentration exceeds that of the catalyst. This suggests that CO_2 binding is not a rate limiting step at high CO_2 concentrations. Peak **b** begins to appear at $[CO_2]$ > 5 mM suggesting that it is related to CO_2 reduction by a species other than $[Ni(cyclam)]^+$. The catalytic current under excess CO_2 and proton source remains peak shaped. This implies that substrate consumption is not the cause of the peak shape but is most likely due to an inhibition process such as catalyst degradation.

Electrochemistry Under CO. Since CO is the major product of the reduction of CO_2 by $[Ni(cyclam)]^{2+}$, the electrochemistry was also studied under CO. The CV of $[Ni(cyclam)]^{2+}$ in a CO saturated 1:4 water:ACN solution (≈6 mM CO) can be seen in Figure 4 (black curve). There is a large positive shift in the Ni(II)/Ni(I) couple under CO relative to N_2 due to CO binding (eq 4). The CO binding constant (K_{co}) calculated from this shift has been reported before in ACN[27] and water[28,29] and is reported in Table 2. The Ni(II)/Ni(I) couple remains reversible under CO if the scan is reversed before −1.3 V. If scanned more negative, an irreversible reduction peak is observed at −1.6 V which is a similar potential as the second catalytic peak, **b**, seen under CO_2. The irreversibility of the second reduction peak in Figure 4 suggests the formation of an unstable Ni(0)(cyclam)(CO) species (eq 5). This formally 20 e^- species is predictably not a stable electronic configuration and could degrade via ligand loss to form more stable Ni(0) carbonyl species. Some of these Ni(0) species may also have CO_2 reduction capabilities. As seen in Figure 4, as CO_2 is incrementally sparged into the solution, this second peak increases in intensity but the peak potential

DOI: 10.1021/ja512575v
J. Am. Chem. Soc. 2015, 137, 3565−3573

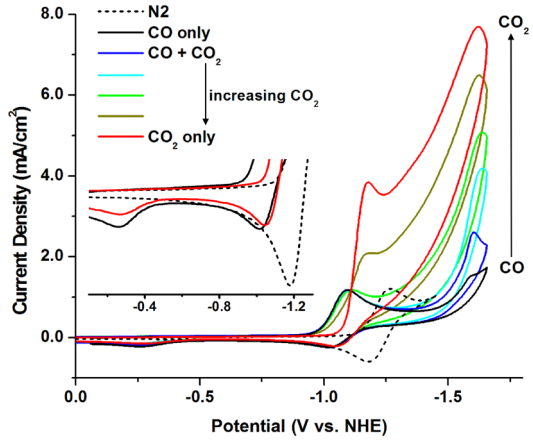

Figure 4. Cyclic voltammograms of 5 mM $[Ni(cyclam)](Cl)_2$, 0.1 M $TBAPF_6$ in 1:4 water:ACN. The solution was saturated with CO (black) and then incrementally sparged with aliquots of CO_2 until saturated (red). Scan rate = 0.1 V/s. Inset: Zoomed region of return oxidation peaks.

remains relatively constant. This implies that this peak is due to the reduction of the same species whether under CO or CO_2. The same reoxidation peaks at ≈ −1 and −0.3 V are present under both CO and CO_2. Similar anodic features were also reported with a Hg working electrode.[28,30] We ascribe the anodic peak at ≈ −1 V to be the oxidation of $[Ni(cyclam)(CO)]^+$ and the anodic peak at ≈ −0.3 V to be the oxidation of a species that forms upon the further reduction $[Ni(cyclam)(CO)]^+$. This species is most likely a Ni(0) carbonyl. This similarity in the CV reduction and oxidation peaks under CO and CO_2 provide strong evidence that one or more stable nickel carbonyl species are formed in the homogeneous reduction of CO_2 at a glassy carbon electrode.

$$[Ni(cyclam)]^+ + CO \rightleftharpoons [Ni(cyclam)(CO)]^+ \quad (4)$$

$$[Ni(cyclam)(CO)]^+ + e^- \rightarrow Ni(0)\text{carbonyl species} \quad (5)$$

IR-SEC. In an effort to identify the nickel carbonyl species, IR spectroelectrochemistry (IR-SEC) experiments were carried out. An IR-SEC cell with a glassy carbon working electrode was constructed in order to match the CV experiments. Figure 5a shows several peaks growing in as the potential is decreased below −1.2 V (vs Ag quasi-reference) under CO_2. The peak at 1955 cm^{-1} is attributed to $[Ni(cyclam)(CO)]^+$ which was verified by doing the same experiment under CO (Figure S2). This $[Ni(cyclam)(CO)]^+$ species has also been observed before by IR at 1955 cm^{-1} in ACN by chemical reduction of $[Ni(cyclam)]^{2+}$ with a Na−Hg amalgam and reaction with CO.[27] The peaks 1666, 1650 (shoulder) and 1615 cm^{-1} that concurrently grow in are assigned as a Ni(II) coordinated bicarbonate species, $[Ni(cyclam)(CO_2OH)]^+$. The IR spectrum of a solution of $[Ni(cyclam)]^{2+}$ and tetraethylammonium bicarbonate in equal concentrations yielded an identical spectrum (Figure S3). No free bicarbonate was seen in the IR-SEC with $[Ni(cyclam)]^{2+}$. The origin of the bicarbonate in this electrocatalytic system is most likely due to CO_2 acting as a Lewis acid toward the expelled OH^- in the CO forming step. This process most likely helps promote the C−OH bond cleavage of the CO_2 adduct. At more negative potentials there is a slight decrease in the 1955, 1666, and 1615 cm^{-1} peaks and a peak at 2042 cm^{-1} grows in. This peak at 2042 cm^{-1} is assigned as $Ni(CO)_4$ by comparison with a genuine sample.

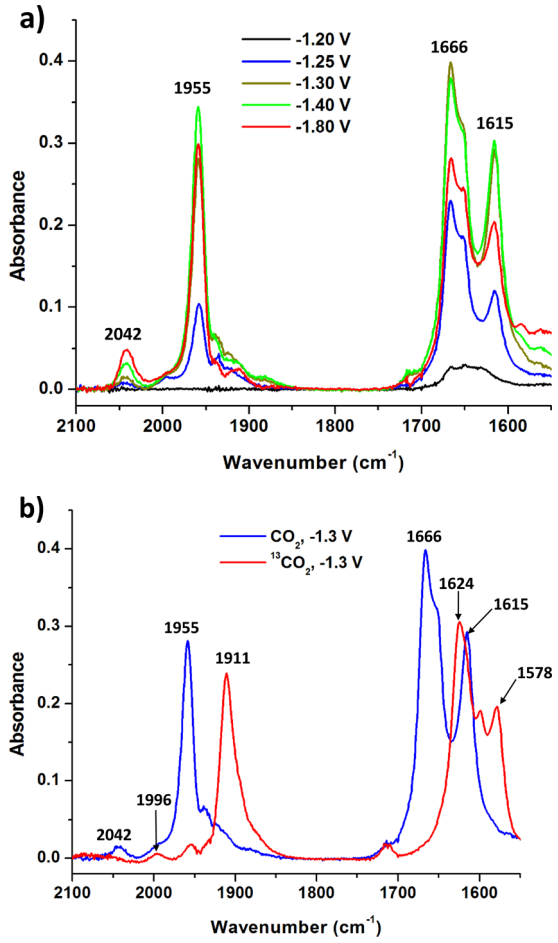

Figure 5. (a) IR-SEC (GC working electrode) of 20 mM of $[Ni(cyclam)](PF_6)_2$ in ACN-d_3 under CO_2. (b) IR-SEC comparing CO_2 and C-13 labeled $^{13}CO_2$.

The same IR-SEC experiment was done using isotopically labeled $^{13}CO_2$ to verify these peaks were arising from reaction with CO_2. The comparison between CO_2 and $^{13}CO_2$ can be seen in Figure 5b. With labeled $^{13}CO_2$ the $[Ni(cyclam)(^{13}CO)]^+$ species shows ν_{CO} at 1911 cm^{-1}. The peaks assigned to $[Ni(cyclam)(^{13}CO_2OH)]^+$ appear at 1624 and 1578 cm^{-1}. $Ni(^{13}CO)_4$ is observed at 1996 cm^{-1}. A summary of the IR peaks can be found in Table 1. The observation of considerable

Table 1. IR Frequencies for Peaks Observed from IR-SEC

assignment	ν_{CO} (cm^{-1})	$\nu^{13}{}_{CO}$ (cm^{-1})	$\Delta\nu$ (cm^{-1})
$[Ni(cyclam)(CO)]^+$	1955	1911	44
$[Ni(cyclam)(CO_2OH)]^+$	1666	1624	42
	1615	1578	37
$Ni(CO)_4$	2042	1996	46

amounts of nickel carbonyl products, $[Ni(cyclam)(CO)]^+$ and $Ni(CO)_4$, in the IR-SEC experiment is clear evidence of catalyst deactivation by the CO produced by the reduction of CO_2. The formation of $[Ni(cyclam)(CO)]^+$ is predicted by the difference in binding and rate constants for CO_2 and CO to $[Ni(cyclam)]^+$ (Table 2). The magnitudes of the CO binding and forward rate constants for eq 4 are ≈10^4 times ≈100 times the corresponding value for CO_2 respectively. These favorable thermodynamic and kinetic parameters for CO binding predict that $[Ni(cyclam)]^+$ will preferentially react with any CO in

DOI: 10.1021/ja512575v
J. Am. Chem. Soc. 2015, 137, 3565−3573

Table 2. Reported Binding Constant (K_L) and Forward (k_f) and Reverse (k_r) Rate Constants for the Binding of Ligand L to [Ni(cyclam)]$^+$

L	solv	K_L (M^{-1})	k_f (M^{-1} s^{-1})	k_r (s^{-1})	ref
CO_2	ACN	4 ± 2			25
	aq.	16	3.2×10^7	2.0×10^6	22
CO	ACN	$(2.8 \pm 0.6) \times 10^5$			27
	aq.	7.5×10^5			28,29
	aq.		$(2 \pm 0.2) \times 10^9$		29
H^+	aq.	60 (pK_a = 1.8)	3×10^7	5×10^5	22

solution and become deactivated toward reaction with CO_2. At more negative potentials the [Ni(cyclam)(CO)]$^+$ formed will be further reduced to generate Ni(0) carbonyl products including $Ni(CO)_4$. Catalytic deactivation by Ni(0) carbonyl products has also been proposed with a Hg electrode.[30]

Addition of a CO Scavenger. With such a high affinity for CO binding, the concentration of the active catalyst [Ni(cyclam)]$^+$ is greatly decreased with each catalyst turnover due to production of CO. In an effort to determine how this catalyst deactivation affects catalytic rates another Ni complex, [Ni(TMC)]$^{2+}$ (TMC = 1,4,8,11-tetramethyl-1,4,8,11-tetraazacyclotetradecane), was used as a CO scavenger. It was shown previously that [Ni(TMC)]$^+$ was not an effective CO_2 reduction catalyst at a glassy carbon electrode.[17] It also has a Ni(II)/Ni(I) reduction potential significantly more positive than [Ni(cyclam)]$^{2+}$ so it does not interfere with the observed catalytic current from the reduction of CO_2 by [Ni(cyclam)]$^+$. Finally, [Ni(TMC)]$^+$ also has a large binding constant for CO, $K_{CO} = (1.2 \pm 0.4) \times 10^5$,[31] to allow it to act as a CO scavenger. Figure 6 shows the effect of the concentration of [Ni(TMC)]$^{2+}$ on the CV of [Ni(cyclam)]$^{2+}$ under CO_2. As [Ni(TMC)]$^{2+}$ is added there are 4 major effects on the voltammogram:

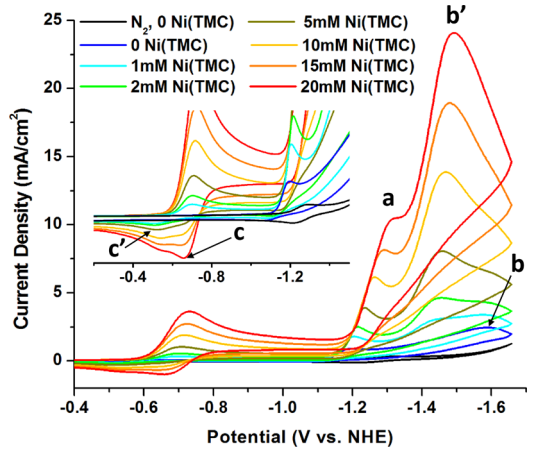

Figure 6. Cyclic voltammograms of 1 mM [Ni(cyclam)](Cl)$_2$, 0.1 M $TBAPF_6$ in 1:4 water:ACN saturated with CO_2 with additions of [Ni(TMC)](Cl)$_2$. Inset: Zoom of oxidation region of [Ni(TMC)]. Scan rate = 0.1 V/s.

(1) The catalytic currents of the two major reduction peaks (**a** and **b**) are increased.

(2) The second catalytic peak **b** is replaced by **b**′. **b** and **b**′ correspond to the reduction of [Ni(cyclam)(CO)]$^+$ and [Ni(TMC)(CO)]$^+$, respectively.

(3) The return oxidation peak of [Ni(TMC)] is shifted from **c**′ to **c**. **c**′ and **c** correspond to the oxidation of [Ni(TMC)(CO)]$^+$ and [Ni(TMC)]$^+$, respectively.

(4) Catalytic peak **a** is shifted negative in potential.

All of these observations are consistent with the [Ni(TMC)]$^+$ acting as a CO scavenger freeing [Ni(cyclam)]$^+$ from deactivation by CO and allowing for higher catalytic currents. The negative shift in peak **a** which accompanies the higher currents can be explained. The addition of the CO scavenger allows for a greater number of catalytic turnovers by [Ni(cyclam)]$^+$. A faster consumption of the local proton source would shift the catalytic peak more negative if a proton dependent electron transfer was becoming the rate limiting step. This is consistent with the data in Figure 2 in which additions of H_2O led to a positive shift in the catalytic peak **a**. The relative rate of catalysis can be determined by measurement of the peak catalytic current (i_{cat}) divided by the peak Faradaic current (i_p) obtained from a CV under CO_2 and N_2 respectively. This ratio (i_{cat}/i_p), though more sophisticated electrochemical methods have been developed recently,[32] is one of the simplest ways to measure the relative catalytic rate. The i_{cat}/i_p of peak **a** in Figure 6 for the various concentrations of [Ni(TMC)]$^{2+}$ can be seen in Table 3. A 10-fold increase is observed at the highest concentration of [Ni(TMC)]$^{2+}$ studied (20 mM).

Table 3. i_{cat}/i_p of Peak a in Figure 6

[Ni(TMC)]$^{2+}$ (mM)	i_{cat}[a] (μA)	i_{cat}/i_p
0	17 (N2)	1
0	55 (CO_2)	3.2
1	108	6.4
2	145	8.5
5	235	13.8
10	364	21.4
15	482	28.4
20	624	36.7

[a]The diffusion current from Ni(TMC)$^{2+}$ was subtracted from the peak to get i_{cat}.

IR-SEC experiments were also conducted with added [Ni(TMC)]$^{2+}$. In Figure 7 a small peak at 1955 cm^{-1} is observed with only 1 mM [Ni(cyclam)]$^{2+}$ under CO_2 as expected. However, when 20 mM [Ni(TMC)]$^{2+}$ is added a much larger peak at 1967 cm^{-1}, which corresponds to [Ni(TMC)(CO)]$^+$, is observed. The species [Ni(TMC)(CO)]$^+$ has been observed by IR at 1967 cm^{-1} previously, generated from chemical reduction of [Ni(TMC)]$^{2+}$ and reaction with CO.[31] The CO that binds to [Ni(TMC)]$^+$ must come from catalytic turnover of [Ni(cyclam)]$^+$ because

DOI: 10.1021/ja512575v
J. Am. Chem. Soc. 2015, 137, 3565−3573

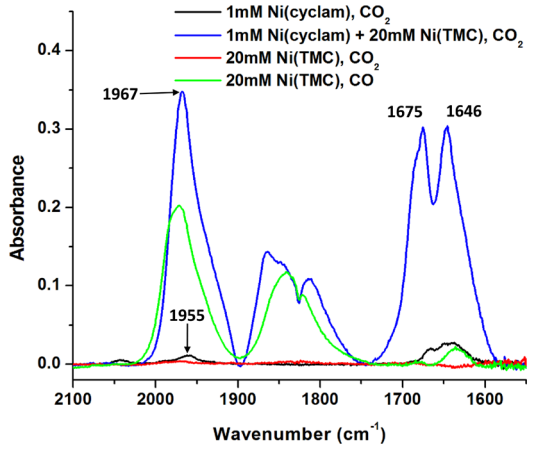

Figure 7. IR-SEC (GC working electrode) of 1 mM of $[Ni(cyclam)](PF_6)_2$ and or 20 mM $[Ni(TMC)](PF_6)_2$ in ACN under CO_2 or CO. Potential = −1.3 V (vs Ag quasi-reference).

no significant peak is observed at 1967 cm^{-1} with only 20 mM $[Ni(TMC)]^{2+}$ under CO_2 at catalytic potentials (red curve in Figure 7). Two peaks at 1675 and 1646 cm^{-1} corresponding to uncoordinated bicarbonate are also observed. The broad peaks observed around 1850 cm^{-1} are assumed to be Ni(0) carbonyl species as they are also observed under CO and only grow in at more negative potentials than the Ni(I) carbonyl species are first observed. This spectral data further supports CO binding to $[Ni(TMC)]^{+}$ under electrocatalytic conditions thereby minimizing the free CO near the electrode surface that would otherwise deactivate the active $[Ni(cyclam)]^{+}$ species (Scheme 2). It would appear that $[Ni(TMC)(CO)]^{+}$ can also form Ni(0) carbonyl species at these potentials.

Scheme 2. Proposed Degradation Pathway of $[Ni(cyclam)]^{2+}$ and Inhibition of Degradation with $[Ni(TMC)]^{+}$ as a CO Scavenger

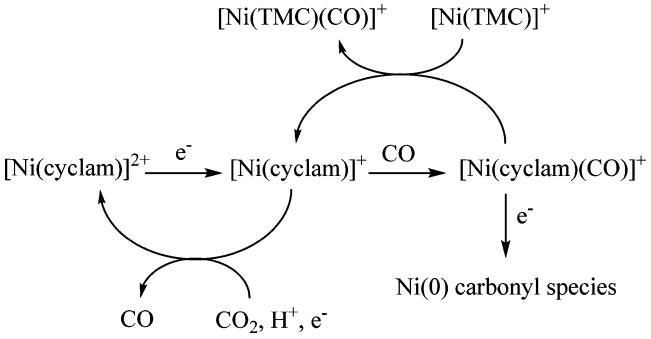

DFT Calculations of the $[Ni(cyclam)(CO)]^{+}$ Structure. There are no examples of crystal structures of nickel tetraazamacrocyclic complexes containing CO as a ligand. Therefore, to understand the favored geometry of such a complex, gas phase density functional theory (DFT) calculations were done using the functional BP86 (more details found in Supporting Information section).

Figure 8 shows the optimized geometry of $[Ni(cyclam)(CO)]^{+}$ for two different isomers, *trans*-I and *trans*-III (Chart 1), which are known to exist in a roughly 15 and 85% equilibrium, respectively, in aqueous solution.[33] It can be seen by the structures in Figure 8 that there are significant distortions to the planar geometry with a bound CO. For

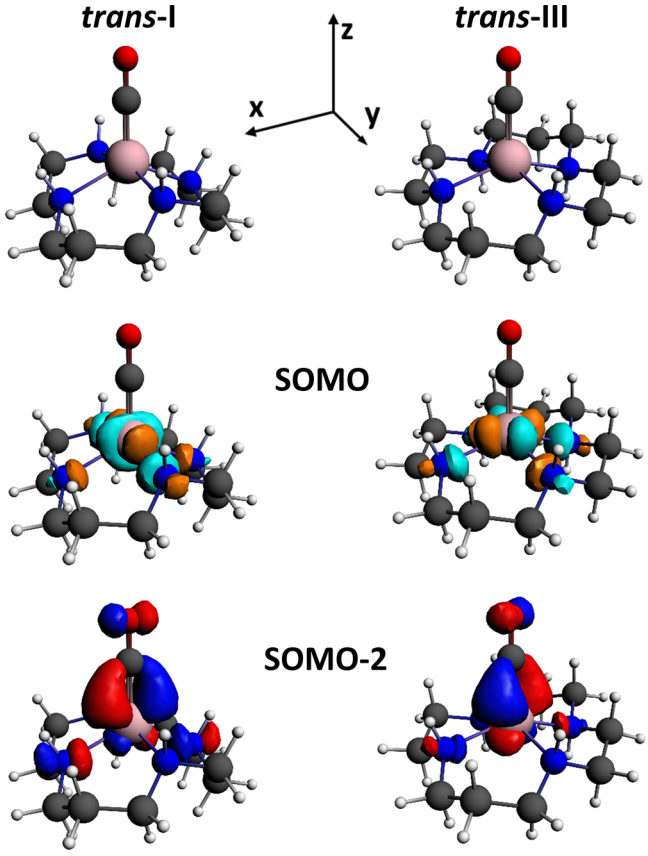

Figure 8. DFT optimized geometries and selected orbitals of $[Ni(cyclam)(CO)]^{+}$ of the *trans*-I and *trans*-III isomers.

Chart 1. Structures of the *trans*-I and *trans*-III Isomers of $[Ni(cyclam)]^{2+}$

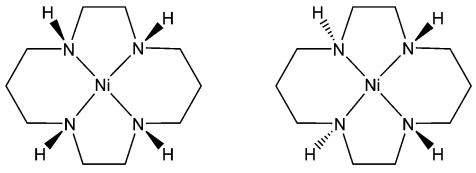

comparison, the DFT optimized structures of $[Ni(cyclam)]^{+}$ only show a slight deviation from planarity with N−Ni−N angles of 176 and 174° for *trans*-I and 179 and 179° for *trans*-III. The different isomers of $[Ni(cyclam)(CO)]^{+}$ distort differently as apparent by the N−Ni−N angles. The *trans*-III structure has a Ni core that is displaced out of the plane of the cyclam nitrogens with nearly equal N−Ni−N angles of 146 and 147°. In the *trans*-I structure, the N−Ni−N angles are 130 and 160° resembling a more trigonal bipyramidal geometry with the CO occupying an equatorial position. This geometry can help stabilize Ni carbonyls by backbonding interactions.[34] The bending of the N−Ni−N angle raises the energy of the d_{xz} and d_{yz} metal orbitals due to overlap with cyclam ligand. This increase in energy allows for better mixing with the π^* of the CO ligand and stronger back-donation and is observed in the SOMO-2 orbital shown in Figure 8. Molecular mechanics calculations have shown that the *trans*-I isomer is more flexible and better suited for out of plane distortions.[35] EXAFS measurements on unsaturated macrocyclic nickel complexes

DOI: 10.1021/ja512575v
J. Am. Chem. Soc. 2015, 137, 3565−3573

also showed out of plane distortions.[27] The *trans*-III structure has roughly equal d_{xz} and d_{yz} orbital energies while the *trans*-I structure has a d_{xz} orbital significantly raised in energy relative to the d_{yz}. The critical angles, bond lengths and relative energies of these DFT structures can be seen in Table 4. The relative

Table 4. Critical Angles and Bond Lengths for DFT Structures Shown in Figure 8

isomer	N−Ni−N angles		avg. Ni−N (Å)	Ni−CO (Å)	ΔE_{CO}[a] (kJ/mol)
trans-I	130°	160°	2.213	1.808	−97
trans-III	146°	147°	2.175	1.821	−67

[a] ΔE_{CO} = CO binding energy. More negative values imply a more favorable bonding interaction. Only the relative difference between the two isomers should be considered.

differences in the CO binding energy (ΔE_{CO}) was modeled by finding the difference in the total bonding energy (TBE) for geometry optimized structures of $[Ni(cyclam)]^+$, $[Ni(cyclam)(CO)]^+$ and free CO and applying eq 6. The absolute energies calculated most likely carry a large error because solvent, counteranions and entropy have been ignored. It is the relative energies between the two isomers that can be of value from these calculations.

$$\Delta E_{CO} = TBE_{[Ni(cyclam)(CO)]^+} - (TBE_{[Ni(cyclam)]^+} + TBE_{CO}) \quad (6)$$

The *trans*-I isomer has a much more favorable CO binding energy relative to the *trans*-III which can also be seen in the shorter Ni−CO bond length for the *trans*-I isomer. Experimental evidence for this conclusion can also be found. A study on the kinetics of addition of CO to $[Ni(cyclam)]^+$ showed a fast addition reaction ($k_{CO} = (2.0 \pm 0.2) \times 10^9$ M^{-1} s^{-1}) followed by a much slower first-order reaction with a rate constant of 1.8 ± 0.2 s^{-1}. The authors ascribed this to an isomerization process from *trans*-III to *trans*-I isomer of $[Ni(cyclam)(CO)]^+$.[29] This would suggest that the *trans*-I form is the more stable isomer once a carbonyl ligand is bound.

It is clear that $[Ni(cyclam)]^+$ forms a stable CO adduct by this DFT calculation and by experiment (high K_{CO}) and that this species is formed in the electrocatalytic reduction of CO_2. By examination of the SOMO of the DFT structures in Figure 8 it can also be seen that reduction of this species places an electron in an orbital that has antibonding character with respect to the Ni−N bonds, thereby weakening these bonds. The $20e^-$ Ni(0)(cyclam)(CO) species would most likely stabilize by N ligand loss. This hypothesis is supported by DFT optimized structures of $[Ni(cyclam)(CO)]^0$, which show significant lengthening of the Ni−N bonds in the *trans*-I structure and cleavage of 2 of the Ni−N bonds in the trans III structure (Figure S4). The Ni(0) carbonyl could then bind more CO (which stabilizes the Ni(0) oxidation state), and eventually total cyclam ligand displacement could be imagined leading to the observed $Ni(CO)_4$ seen in the IR-SEC experiments. All of these results are consistent with the deactivation of $[Ni(cyclam)]^+$ by CO at negative potentials.

Comparison with Catalysis on Mercury. The wealth of data of the CO_2 reduction by $[Ni(cyclam)]^{2+}$ at a Hg electrode can be used to compare with the present results at an inert glassy carbon electrode. It has been established that $[Ni(cyclam)]^+$ is absorbed onto the Hg surface and this species differs in electrocatalytic properties compared to the non-adsorbed species. Very large i_{cat}/i_p values are obtained at low catalyst concentrations with an Hg electrode.[14] However, this current quickly drops to near zero as the potential is scanned more negative due to formation of insoluble Ni(0) carbonyl species, which block the electrode from adsorption of the active $[Ni(cyclam)]^+$ catalytic species.[30] The formation of a $[Ni(cyclam)(CO)]^+$ species during CO_2 reduction has been observed with a Hg electrode.[14] However, there are two major differences with the catalytic behavior of $[Ni(cyclam)]^+$ when adsorbed on Hg as compared to the homogeneous system described here. First, the positive shift in potential of the onset of the catalytic current under CO_2 vs the onset of the Faradaic current under N_2 is much greater for Hg (≈300 mV)[14] than glassy carbon (≈40 mV). This is because the Hg surface stabilizes the reductively adsorbed complex allowing the catalytically active Ni(I) redox state to be achieved at a much more positive potential than the Ni(II/I) couple in solution.[16] Second, the initial catalytic rates are much faster on Hg than glassy carbon (without added CO scavenger). The current results here would suggest that the major limitation to higher catalytic currents in the homogeneous system is deactivation of the catalyst by CO. It would stand to reason that perhaps when adsorbed on Hg, the deactivation of catalysis initiated by CO binding would be attenuated. The reason for this decline in CO binding could be due to the constraint of the macrocyclic ligand to bend out of a square planar geometry. As shown by our DFT results, If the cyclam ring is allowed to bend along one or both of the N−Ni−N angles to <180°, then the CO adduct will be stabilized. To further illustrate this stabilization effect, an additional DFT calculation was done for $[Ni(cyclam)(CO)]^+$ with constraints on the N−Ni−N angles to remain unchanged from the $[Ni(cyclam)]^+$ optimized structure (176, 174° and 179, 179° for *trans*-I and *trans*-III, respectively). The *trans*-I angle-constrained structure had a ΔE_{CO} that was 47 kJ/mol higher (destabilized) relative to the non angle-constrained structure in Figure 8. A geometry converged structure of the *trans*-III $[Ni(cyclam)(CO)]^+$ was not reached with these angle-constraints instead favoring breaking of the Ni−CO bond. This DFT result emphasizes the necessity for the bending out of square planar geometry to achieve a highly stable CO adduct. If the Hg surface prevents such a distortion of the square planar cyclam ligand then this stabilization of the $[Ni(cyclam)(CO)]^+$ might be prevented and could lead to increased catalytic rates relative to what is seen without Hg. Addition of the CO scavenger in the heterogeneous system, in effect, helps to minimize the formation of the $[Ni(cyclam)(CO)]^+$ in the first place.

The true identity of the adsorbed species on Hg still remains unclear. Hg could lend electronic effects that encourage CO_2 binding.[36,37] An increased CO_2 binding constant for the adsorbed species would lead to higher TOF because CO_2 could better compete with CO for binding to the Ni(I) metal center. Some reports hypothesize that the adsorbed species is in the *trans*-I geometry and that this isomer has increased CO_2 reduction activity.[15] Past computational reports support that *trans*-I has a higher affinity for CO_2 binding in gas phase[17] and solvated.[38] However, no difference was observed in the rate of reductive adsorption on Hg of a freshly prepared solution of recrystallized $[Ni(cyclam)]2^+$ (which is all *trans*-III) and an aged solution (15% *trans*-I).[16] The authors concluded that the *trans*-I isomer is not the species responsible for the unusual reductive adsorption of $[Ni(cyclam)]^+$. Whether or not the isomeric form of $[Ni(cyclam)]^+$ has an effect on the catalytic

DOI: 10.1021/ja512575v
J. Am. Chem. Soc. 2015, 137, 3565−3573

reduction of CO_2 has not been thoroughly established experimentally. However, its importance to the catalytic activity must be considered. Isomerization can be base catalyzed, operating with a deprotonation of the amine proton on the cyclam ring followed by inversion.[33] These basic conditions are met by examination of the overall electrocatalytic reaction of $[Ni(cyclam)]^{2+}$ with CO_2 in the presence of water (or other weak acid) (eq 7). Clearly there will be a local increase in pH near the electrode surface due to proton consumption and generation of OH^- (or other conjugate base). Alternatively, it has been reported that reduction of some Ni(II) complexes is accompanied, or followed by, isomerization processes.[23] Therefore, under electrocatalytic conditions, the barrier to isomerization might be rather low. More experimental work will be needed to determine if an isomerization process is important to the catalytic activity of CO_2 reduction—and if so—is it beneficial or detrimental to the prolonged turnover of the catalyst? The DFT results here suggest that an isomerization is a possible pathway to catalyst deactivation by formation of a more stable $[Ni(cyclam)(CO)]^+$ species.

$$[Ni(cyclam)]^{2+} + 2e^- + CO_2 + H_2O \rightarrow [Ni(cyclam)]^{2+} + CO + 2OH^- \quad (7)$$

CONCLUSION

$[Ni(cyclam)]^{2+}$ has proven to be a fast, efficient and selective catalyst for the reduction of CO_2 to CO. The species $[Ni(cyclam)(CO)]^+$ was observed in appreciable quantities during CO_2 reduction by CV and IR-SEC. At more negative potentials, $Ni(CO)_4$ was also observed. These results lead to the assumption that catalyst deactivation by CO is a major limitation to higher catalytic currents. This assumption was supported by the addition of another macrocyclic Ni complex, $[Ni(TMC)]^{2+}$, to act as a CO scavenger. Addition of $[Ni(TMC)]^{2+}$ leads to a substantial increase (up to 10 times) in the catalytic current observed in a CV. Observation of $[Ni(TMC)(CO)]^+$ by IR-SEC supports the role of the reduced $[Ni(TMC)]^+$ species as a CO scavenger to allow for $[Ni(cyclam)]^+$ to remain in its active state. DFT calculations were done on the *trans*-I and *trans*-III isomers of the $[Ni(cyclam)(CO)]^+$ species. There is significant out-of-plane distortion observed in both isomers but the *trans*-I structure favored a geometry with an extreme angle on only one of the N—Ni—N bonds approaching a more trigonal bipyramidal geometry with the CO ligand in a equatorial position. The $[Ni(cyclam)(CO)]^+$ species can be further reduced to Ni(0) carbonyl species, which may degrade by cyclam ligand loss, especially in the presence of excess CO.

The results of this report suggest that the higher peak current densities on Hg are due to suppression of the degradation pathway toward Ni(0) carbonyl species. Even though Ni(0) carbonyl species were observed on a Hg electrode and thought to inhibit catalysis, the CO_2 reduction at a Hg electrode occurs at a much more positive potential than Ni(0) species can be formed. Therefore, very high catalytic currents can be observed at these more positive potentials. The adsorbed species is likely to have increased energy barriers for loss of planarity of the cyclam ring. The folding and eventual loss of one or multiple N—Ni bonds of the cyclam ligand is a probable degradation path at negative potentials leading to Ni(0) species with strong affinity for CO. This self-poisoning behavior is presumed to be minimized by interaction of the complex with the Hg surface. However, the hypothesis that the Hg surface acts to stabilize a more planar geometry of cyclam complexes that more readily releases CO remains to be verified experimentally or computationally.

ASSOCIATED CONTENT

Supporting Information

Figures S1—S4 and synthetic and DFT details. This material is available free of charge via the Internet at http://pubs.acs.org.

AUTHOR INFORMATION

Corresponding Author

ckubiak@ucsd.edu

Notes

The authors declare no competing financial interest.

ACKNOWLEDGMENTS

Thanks to Matt Sampson and all of the Pubsketballers. Thanks to Prof. Figueroa for assistance with DFT calculations. This material is based upon work supported by the Air Force Office of Scientific Research through the MURI program under AFOSR Award No. FA9550-10-1-0572.

REFERENCES

(1) Appel, A. M.; Bercaw, J. E.; Bocarsly, A. B.; Dobbek, H.; DuBois, D. L.; Dupuis, M.; Ferry, J. G.; Fujita, E.; Hille, R.; Kenis, P. J. A.; Kerfeld, C. A.; Morris, R. H.; Peden, C. H. F.; Portis, A. R.; Ragsdale, S. W.; Rauchfuss, T. B.; Reek, J. N. H.; Seefeldt, L. C.; Thauer, R. K.; Waldrop, G. L. *Chem. Rev.* **2013**, *113*, 6621.
(2) Qiao, J.; Liu, Y.; Hong, F.; Zhang, J. *Chem. Soc. Rev.* **2014**, *43*, 631.
(3) Berardi, S.; Drouet, S.; Francas, L.; Gimbert-Surinach, C.; Guttentag, M.; Richmond, C.; Stoll, T.; Llobet, A. *Chem. Soc. Rev.* **2014**, *43*, 7501.
(4) Hori, Y.; Wakebe, H.; Tsukamoto, T.; Koga, O. *Electrochim. Acta* **1994**, *39*, 1833.
(5) Kedzierzawski, P.; Augustynski, J. *J. Electrochem. Soc.* **1994**, *141*, L58.
(6) Savéant, J.-M. *Chem. Rev.* **2008**, *108*, 2348.
(7) Benson, E. E.; Kubiak, C. P.; Sathrum, A. J.; Smieja, J. M. *Chem. Soc. Rev.* **2009**, *38*, 89.
(8) Windle, C. D.; Perutz, R. N. *Coord. Chem. Rev.* **2012**, *256*, 2562.
(9) Costentin, C.; Robert, M.; Saveant, J.-M. *Chem. Soc. Rev.* **2013**, *42*, 2423.
(10) Bourrez, M.; Molton, F.; Chardon-Noblat, S.; Deronzier, A. *Angew. Chem., Int. Ed.* **2011**, *50*, 9903.
(11) Smieja, J. M.; Sampson, M. D.; Grice, K. A.; Benson, E. E.; Froehlich, J. D.; Kubiak, C. P. *Inorg. Chem.* **2013**, *52*, 2484.
(12) Costentin, C.; Drouet, S.; Robert, M.; Savéant, J.-M. *Science* **2012**, *338*, 90.
(13) Fisher, B. J.; Eisenberg, R. *J. Am. Chem. Soc.* **1980**, *102*, 7361.
(14) Beley, M.; Collin, J. P.; Ruppert, R.; Sauvage, J. P. *J. Am. Chem. Soc.* **1986**, *108*, 7461.
(15) Schneider, J.; Jia, H.; Kobiro, K.; Cabelli, D. E.; Muckerman, J. T.; Fujita, E. *Energy Environ. Sci.* **2012**, *5*, 9502.
(16) Balazs, G. B.; Anson, F. C. *J. Electroanal. Chem.* **1992**, *322*, 325.
(17) Froehlich, J. D.; Kubiak, C. P. *Inorg. Chem.* **2012**, *51*, 3932.
(18) Wilhelm, E.; Battino, R.; Wilcock, R. J. *Chem. Rev.* **1977**, *77*, 219.
(19) Fujita, E.; Creutz, C.; Sutin, N.; Szalda, D. J. *J. Am. Chem. Soc.* **1991**, *113*, 343.
(20) Tomita, Y.; Teruya, S.; Koga, O.; Hori, Y. *J. Electrochem. Soc.* **2000**, *147*, 4164.
(21) Machan, C. W.; Sampson, M. D.; Chabolla, S. A.; Dang, T.; Kubiak, C. P. *Organometallics* **2014**, *33*, 4550.

DOI: 10.1021/ja512575v
J. Am. Chem. Soc. 2015, 137, 3565—3573

(22) Kelly, C. A.; Mulazzani, Q. G.; Venturi, M.; Blinn, E. L.; Rodgers, M. A. J. *J. Am. Chem. Soc.* **1995**, *117*, 4911.
(23) Zilbermann, I.; Winnik, M.; Sagiv, D.; Rotman, A.; Cohen, H.; Meyerstein, D. *Inorg. Chim. Acta* **1995**, *240*, 503.
(24) Gagne, R. R.; Allison, J. L.; Ingle, D. M. *Inorg. Chem.* **1979**, *18*, 2767.
(25) Fujita, E.; Haff, J.; Sanzenbacher, R.; Elias, H. *Inorg. Chem.* **1994**, *33*, 4627.
(26) Song, J.; Klein, E. L.; Neese, F.; Ye, S. *Inorg. Chem.* **2014**, *53*, 7500.
(27) Furenlid, L. R.; Renner, M. W.; Szalda, D. J.; Fujita, E. *J. Am. Chem. Soc.* **1991**, *113*, 883.
(28) Fujihira, M.; Hirata, Y.; Suga, K. *J. Electroanal. Chem. Interfacial Electrochem.* **1990**, *292*, 199.
(29) Kelly, C. A.; Mulazzani, Q. G.; Blinn, E. L.; Rodgers, M. A. J. *Inorg. Chem.* **1996**, *35*, 5122.
(30) Balazs, G. B.; Anson, F. C. *J. Electroanal. Chem.* **1993**, *361*, 149.
(31) Szalda, D. J.; Fujita, E.; Sanzenbacher, R.; Paulus, H.; Elias, H. *Inorg. Chem.* **1994**, *33*, 5855.
(32) Costentin, C.; Drouet, S.; Robert, M.; Savéant, J.-M. *J. Am. Chem. Soc.* **2012**, *134*, 11235.
(33) Connolly, P. J.; Billo, E. J. *Inorg. Chem.* **1987**, *26*, 3224.
(34) Macgregor, S. A.; Lu, Z.; Eisenstein, O.; Crabtree, R. H. *Inorg. Chem.* **1994**, *33*, 3616.
(35) Thom, V. J.; Fox, C. C.; Boeyens, J. C. A.; Hancock, R. D. *J. Am. Chem. Soc.* **1984**, *106*, 5947.
(36) Sakaki, S. *J. Am. Chem. Soc.* **1990**, *112*, 7813.
(37) Sakaki, S. *J. Am. Chem. Soc.* **1992**, *114*, 2055.
(38) Schneider, J.; Jia, H.; Muckerman, J. T.; Fujita, E. *Chem. Soc. Rev.* **2012**, *41*, 2036.

DOI: 10.1021/ja512575v
J. Am. Chem. Soc. 2015, 137, 3565−3573